Paper title: Pulmonary lobar segmentation from computed tomography scans based on a statistical finite element analysis of lobe shape

Authors: Yuwen Zhang[1], Mahyar Osanlouy[1], Alys R. Clark[1], Hari Kumar[1], Margaret L. Wilsher[2], David G. Milne[2], Eric A. Hoffman [3], Merryn H. Tawhai[1]

[1]Auckland Bioengineering Institute, University of Auckland, Auckland, NZ, [2]Auckland City Hospital, Auckland District Health Board, Auckland, NZ, [3]Department of Radiology and Biomedical Engineering, University of Iowa, Iowa City, IA, USA.

250-word abstract text:
Automatic identification of pulmonary lobes from imaging is important in disease assessment and treatment planning. However, the lobar fissures can be difficult to detect automatically, as they are thin, usually of fuzzy appearance and incomplete. The fissures can also be obscured by or confused with features of disease, for example the tissue abnormalities that characterise fibrosis. Traditional anatomical knowledge-based methods rely heavily on anatomic knowledge and largely ignore individual variability, which may result in failure to segment pathological lungs. In this study, we aim to overcome difficulties in identifying pulmonary fissures by using a statistical finite element shape model of lobes to guide lobar segmentation. By deforming a principle component analysis based statistical shape model onto an individual's lung shape, we predict the likely region of fissure locations, to initialize the search region for fissures. Then, an eigenvalue of Hessian matrix analysis and a connected component eigenvector based analysis are used to determine a set of fissure-like candidate points. A smooth multi-level β-spline curve is fitted to the most fissure-like points (those with high fissure probability) and the fitted fissure plane is extrapolated to the lung boundaries. The method was tested on 20 inspiratory and expiratory CT scans, and the results show that the algorithm performs well both in healthy young subjects and older subjects with fibrosis. The method was able to estimate the fissure location in 100% of cases, whereas two comparison segmentation softwares that use anatomy-based methods were unable to segment 7/20 and 9/20 subjects, respectively.

Description of purpose:
Identification of pulmonary lobes in imaging is important for assessment of lung disease severity and treatment planning. The lobes act somewhat independently of each other with respect to respiratory function, thus many pulmonary diseases act at a lobar level. For clinical applications, identification of the pulmonary fissures can be an important step in the image-based study of lung function and disease: knowing the lobar distribution of pulmonary disease is beneficial for clinicians to recognize pathogenesis and guide therapy. However, the lobes are difficult to segment automatically as they can appear as faint or fuzzy lines in imaging, fissures can be incomplete (even in healthy patients), and there is anatomical variation in lobe shape and size between individuals. Current published anatomy-based methods rely heavily on anatomic knowledge, thus often fail to perform well in pathological lungs. In this study, we aim to develop a statistical shape model guided lobe segmentation method to overcome difficulties in identifying pulmonary fissures.

Methods:
1. Lung Segmentation
A commonly used thresholding method is used to segment the lungs.

2. Statistical finite element models of lung and fissure shape
To guide fissure detection, a statistical shape model (SSM) based on an active shape model (ASM) of the lung was derived from a training set of segmented lung and fissure surface locations. The training set consisted of data from 50 healthy non-smokers that was retrospectively selected from two independent but consistent imaging studies (following institutional and regional ethics approval for each study). A high order (bi-cubic Hermite) finite element surface mesh with the same mesh connectivity for each subject was used to describe the shape of the lung and its fissures in terms of the ASM.
To construct the SSM, the location and derivatives at each node (landmark or pseudo-landmark) in

the finite element mesh was used in a principal component analysis (PCA) conducted on the training set. To remove orientation and scaling differences between shapes, a general procrustes alignment (GPA) method was used to minimize the distance between subject meshes through calculating an optimal rotation matrix and translation, then the volume of all subjects was normalized. The procrustes aligned mesh was represented by

$$S = [\overline{x_1}\ \overline{y_1}\ \overline{z_1}\ \overline{x_2}\ \overline{y_2}\ \overline{z_2} \cdots \overline{x_p}\ \overline{y_p}\ \overline{z_p}],$$

where p is the total number of nodes of all the subjects, and the over-line represents GPA to the mean. The matrix S was decomposed into modes of shape variation by a PCA. Each mode represents one type of lung and fissure surface shape variation. The first seven principal components accounted for over 90% of the total variation in the training set. Lung and lobe SSM were constructed separately, based on PCA.

3. Initial prediction of lobar location in an individual

A finite element mesh of the lung surface (i.e. without fissure information) was generated for a new subject (a subject who was not part of the training set). This lung surface mesh was projected on to the lung SSM (i.e. with no fissure surfaces). The principal component weight values were calculated from the projection and these weights were used to deform the lobe SSM that contained both lung and fissure surfaces to the subject, to give an initial estimation of fissure locations.

4. Multiscale Hessian-based fissure detection

The location of the SSM predicted fissure planes were used to guide a Hessian based fissure detection in an individual. Gaussian filters with kernel sizes from 0.5-2.5 mm in 0.5 mm increments were applied to the image set. The responses at each kernel were combined to get a maximum response for each voxel of the image. At each image voxel, the Hessian matrix was constructed as a symmetric matrix. Because a fissure structure presents as a light plane on a dark background, the relationship of eigenvalues λ_1, λ_2, λ_3 of Hessian were defined as $|\lambda_1| \leq |\lambda_2| \leq |\lambda_3|$. A filter was developed to give a high response to local sheet-like structures (fissures) and to suppress other pulmonary structures. An example of this filter applied in an individual is shown in Fig 1(a). Blood vessels, which appear as similar structures locally to fissures, were removed from the fissure enhanced result using previously described methods, which removes tube-like structures (vessels) with $|\lambda_1| \approx 0$, $|\lambda_1| \ll |\lambda_2|$, $|\lambda_2| \approx |\lambda_3|$ (Fig 1(b)).

The fissure location predicted by SSM deformation allows definition of a search region for the fissure (Fig 1(c)). A 2D 4-neighborhood connected component filter and a 3D 6-neighborhood vector-based connected component filter were employed successively to eliminate noise arising from small plane-like structures in this search region (Fig 1(d)). The vector-based connected component filter used the inner product of the normalized largest eigenvector of the Hessian in adjacent voxels.

The detected points were then divided into a set of small subsections corresponding to different x, y intervals. For each subsection, the point of the highest fissure probability was selected as the final candidate fissure point (Fig 1(e)). Then a continuous smooth fissure surface was generated using a β-spline method with a thin-plane spline and extrapolated to the lung boundaries, see Fig 1(f).

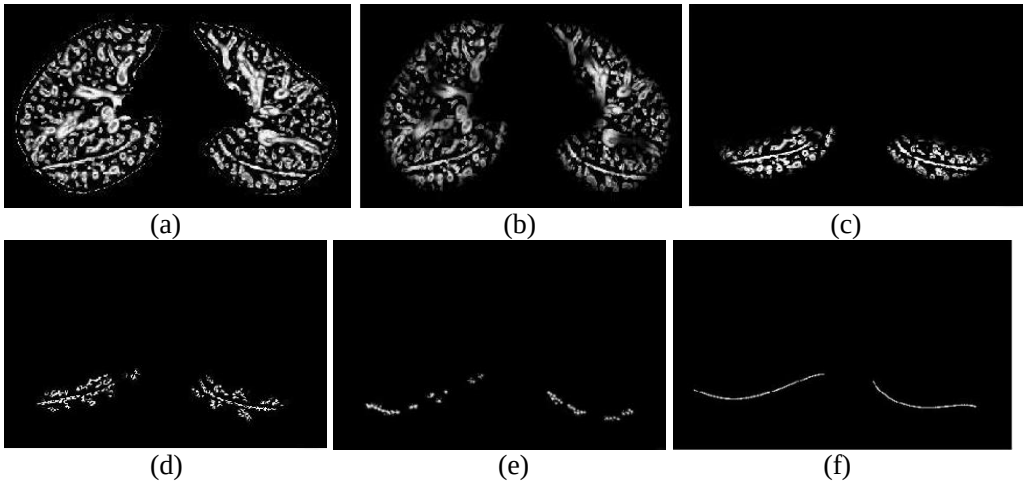

Fig. 1. Hessian-based multiscale fissure detection results. (a) Hessian-based fissure enhancement. (b) Remove vessel voxels. (c) ROI of fissure locations based on SSM projection. (d) 2D and 3D eigenvector based connected component filter. (e) Fissure candidate points. (f) B-spline curve fissure surface fitting.

Results:
The method was tested on 20 inspiratory and expiratory CT scans: 10 healthy young subjects and 10 older subjects diagnosed with idiopathic pulmonary fibrosis (IPF). Slice thickness was 0.5-3.0mm. To quantitatively assess the accuracy of the lobar segmentation method, the segmentation results were compared with 'gold-standard' manual segmentations. Segmentation accuracy was quantitatively evaluated by computing the mean difference and percentage of fissure points <3 mm between the gold-standard and semi-automatic method. The quantitative evaluation is shown in Table 1.
The ability of the method to provide an initial estimate of the fissure locations was compared with two other segmentation softwares which use watershed-based (anatomical knowledge-based) methods. The two segmentation softwares were unable to segment 7/20 and 9/20 subjects respectively (1/10 and 2/10 normal, and 6/10 and 7/10 IPF subjects). In contrast, the model-based method can estimate the fissure location for all subjects at all volumes.
Fig 2 shows the spatial distribution of error for three representative subjects. Error was highest in regions close to the hilum (where the anatomical structures are complex, and/or the fissure is often incomplete), and where the right fissures meet.

New or breakthrough work to be presented:
We presented a statistical finite element shape model-guided method to segment pulmonary lobes from CT images. This new procedure does not depend on prior segmentation of anatomical structures (airway lobar classification) therefore can provide a relatively accurate lobe segmentation result in all cases (including normal and abnormal cases), whereas some published methods fail to estimate fissures in pathological lungs or even fail in normal lungs.

Table 1: Mean error and percentile accuracy of normal healthy and IPF subjects (average value ± standard deviation).

	Normal healthy subjects		IPF subjects	
	Mean error(mm)	Accuracy (%)	Mean error(mm)	Accuracy (%)
Left oblique	1.76 ± 0.68	81.19 ± 6.61	2.82 ± 0.71	70.26 ± 9.10
Right horizontal	3.66 ± 1.37	64.81 ± 13.19	5.39 ± 1.90	58.43 ± 14.53
Right oblique	2.55 ± 0.90	73.81 ± 7.96	4.71 ± 1.60	62.86 ± 11.21

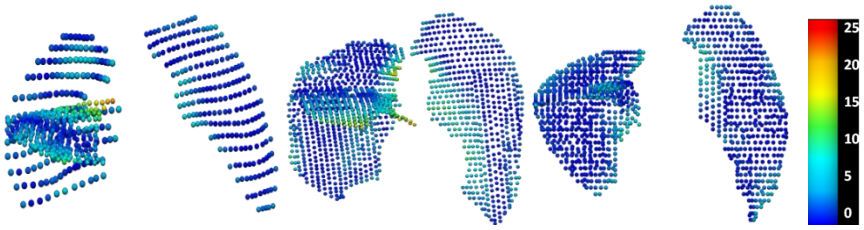

(a) (b) (c)

Fig. 2. The spatial distribution of error between the gold-standard and semi-automatic methods for three representative subjects, highlighting localized regions of low accuracy.

Conclusions:
In this study, we developed a pulmonary lobar segmentation method. Results show that the method can perform well to detect the location of the fissures over most of the fissure surfaces on CT images from normal subjects, and provides a relatively accurate result for IPF (abnormal) subjects although manual interaction is still needed for a few subjects. This method has promising potential as a clinically useful semi-automatic lobe segmentation procedure.

Whether the work is being, or has been, submitted for publication or presentation elsewhere:
No